

Lifetime measurements probing collectivity in the ground-state band of ^{32}Mg

R. Elder¹, H. Iwasaki^{2,3}, J. Ash^{2,3}, D. Bazin^{2,3}, P. C. Bender^{2,4}, T. Braunroth⁵, C. M. Campbell⁶, H. L. Crawford⁶, B. Elman^{2,3}, A. Gade^{2,3}, M. Grinder^{2,3}, N. Kobayashi⁷, B. Longfellow^{2,3}, T. Mijatović^{2,8}, J. Pereira², A. Revel², D. Rhodes^{2,3} and D. Weisshaar²

¹*Department of Physics and Engineering, Washington and Lee University, Lexington, Virginia 24450, USA*

²*National Superconducting Cyclotron Laboratory, Michigan State University, East Lansing, Michigan 48824, USA*

³*Department of Physics and Astronomy, Michigan State University, East Lansing, Michigan 48824, USA*

⁴*Department of Physics, University of Massachusetts Lowell, Lowell, Massachusetts 01854, USA*

⁵*Institut für Kernphysik, Universität zu Köln, 50937 Köln, Germany*

⁶*Nuclear Science Division, Lawrence Berkeley National Laboratory, Berkeley, California 94720, USA*

⁷*Research Center for Nuclear Physics, Osaka University, Ibaraki, Osaka 567-0047, Japan*

⁸*Ruđer Bošković Institute, HR-10 002 Zagreb, Croatia*



(Received 21 May 2021; accepted 9 July 2021; published 4 August 2021)

The signatures of inversion between normal and intruder configurations of particle-hole excitations across the $N = 20$ shell gap in the neutron-rich isotope ^{32}Mg have long been of keen interest. Electromagnetic transition rates in the ground-state band are key quantities that provide insights into collective properties associated with the contributions of the 2p2h and 4p4h intruder configurations. The combination of TRIPLEX, GRETINA, and the S800 spectrograph enables model-independent lifetime measurements to determine electromagnetic transition rates in rare isotopes. The reduced $E2$ transition rates in ^{32}Mg between the 2_1^+ and 0_1^+ states and between the 4_1^+ and 2_1^+ states have been measured, the latter representing the first experimental $B(E2)$ value for this transition. The $B(E2)$ strengths indicate large collectivity and strong contributions from the 2p2h and 4p4h intruder configurations that may change with spin in the ground-state band of ^{32}Mg .

DOI: [10.1103/PhysRevC.104.024307](https://doi.org/10.1103/PhysRevC.104.024307)

I. INTRODUCTION

The neutron-rich isotope ^{32}Mg has long been associated with the $N = 20$ island of inversion, a region where the conventional magic number that is valid near stability breaks down [1]. Near the stable isotopes, nuclides with $N = 20$ neutrons are dominated by the configuration that fills the sd shell and leaves the pf shell unoccupied, which is referred to as the *normal* configuration. In ^{32}Mg and other nearby neutron-rich nuclides, the ground-state band is understood to be dominated instead by deformation-driving *intruder* configurations such as the two-particle-two-hole (2p2h) and four-particle-four-hole (4p4h) configurations that involve the promotion of two and four neutrons, respectively, across the reduced sd - pf shell gap. The ^{32}Mg nuclide exhibits several characteristics that provide evidence for the collectivity that results from the intruder configurations, such as excess binding energy [2], reduced $E(2_1^+)$ [3], energy spacing of the known yrast states up to 6^+ being consistent with a deformed shape [4,5], and an enhanced $B(E2)$ value between the 0_1^+ ground state and the 2_1^+ first-excited state [6–12].

Although the $N = 20$ island of inversion has been studied for decades, details of the mixing among normal and intruder configurations in ^{32}Mg are still being explored. Recent studies of the 0_2^+ state excitation energy, cross section, and lifetime have suggested that this state has strong contributions from the 2p2h and 4p4h intruder configurations [13–15]. A natural

question is, “how are the strengths of the $0p0h$, 2p2h, and 4p4h configurations divided between the 0_1^+ and 0_2^+ states and the associated band structures?” While there is evidence for collectivity in the ground-state band driven by the intruder configurations [2–12], the particular balance of the 2p2h, 4p4h, and possibly higher-order intruder configurations is insufficiently understood. A shell-model study has shown that the $B(E2)$ values vary considerably whether pure $0p0h$, 2p2h, or 4p4h configurations are assumed for the ground-state band of ^{32}Mg [16]. This suggests that a robust understanding of the transition strengths in ^{32}Mg can improve our understanding of the relative contributions among these configurations.

Several experiments have studied the collectivity of ^{32}Mg by measuring the $B(E2; 0_1^+ \rightarrow 2_1^+)$ value, but the results vary considerably by about a factor of two. The first result came from an intermediate-energy Coulomb excitation reaction which found $B(E2; 0_1^+ \rightarrow 2_1^+) = 454(78) e^2 \text{fm}^4$ [6] and was consistent with an available shell-model calculation that included both sd and pf shells [17]. The next reported measurement found $B(E2; 0_1^+ \rightarrow 2_1^+) = 440(55) e^2 \text{fm}^4$ [7] before applying feeding corrections, which was consistent with the first measurement. Two subsequent results disagreed with one another, one reporting a considerably larger value of $B(E2; 0_1^+ \rightarrow 2_1^+) = 622(90) e^2 \text{fm}^4$ [8], and the other reporting $B(E2; 0_1^+ \rightarrow 2_1^+) = 449(53) e^2 \text{fm}^4$ [9], in good agreement with the original measurement. Later Coulomb

excitation results [10,11] did not reproduce the larger value reported by Ref. [8], appearing to confirm the $B(E2)$ value to be about $450 e^2 \text{fm}^4$. However, the feeding corrections applied in the past Coulomb excitation results have varied from 5% to 25% [6–8,10,11], broadening the range of published data to as low as $B(E2; 0_1^+ \rightarrow 2_1^+) = 328(48) e^2 \text{fm}^4$, as deduced in Ref. [10]. The only lifetime measurement of the 2_1^+ state is based on the fast-timing method and results in $B(E2; 0_1^+ \rightarrow 2_1^+) = 327(87) e^2 \text{fm}^4$ [12], closest to the lowest value reported by Coulomb-excitation studies, but in agreement within 1σ with all but the largest Coulomb excitation results.

The variation among the past experimental $B(E2; 0_1^+ \rightarrow 2_1^+)$ values by about a factor of two should be resolved to provide a clear depiction of the structure in the ^{32}Mg ground-state band. Theoretical predictions for ^{32}Mg that include the pf shell are able to demonstrate an increase in $B(E2; 0_1^+ \rightarrow 2_1^+)$ from ^{30}Mg to ^{32}Mg [16,18–22]. These predicted $B(E2; 0_1^+ \rightarrow 2_1^+)$ values for ^{32}Mg vary by only about 20%, so to make a useful comparison with data the variance in the measured results ought to be reduced. The recoil-distance method can provide a model-independent lifetime measurement to improve the precision of the $B(E2; 0_1^+ \rightarrow 2_1^+)$ value [23], and resolve the discrepancy among the past results which were mostly from intermediate-energy Coulomb excitation experiments.

The 4_1^+ state merits a direct lifetime measurement as well. No measurement of the $B(E2)$ value between the 2_1^+ and 4_1^+ states has yet been made. This $B(E2)$ value is important to provide additional insight into the collective interpretation of the ground-state band that is suggested by the energy spacing of the yrast states [5]. Assuming the expected ratio of $B(E2)$ values in an axially deformed band of $B(E2; 4_1^+ \rightarrow 2_1^+)/B(E2; 2_1^+ \rightarrow 0_1^+) = 1.43$ and a $B(E2; 2_1^+ \rightarrow 0_1^+)$ estimated to be $91 e^2 \text{fm}^4$ from the measurements discussed above [24], the $B(E2; 4_1^+ \rightarrow 2_1^+)$ should be $130 e^2 \text{fm}^4$. This corresponds to a 4_1^+ lifetime estimate of $\tau = 1.0$ ps. Alternatively, for a vibrational band the expected ratio is $B(E2; 4_1^+ \rightarrow 2_1^+)/B(E2; 2_1^+ \rightarrow 0_1^+) = 2.0$, leading to a $B(E2; 4_1^+ \rightarrow 2_1^+) = 182 e^2 \text{fm}^4$ and a lifetime of $\tau = 0.7$ ps. A measurement of $B(E2; 4_1^+ \rightarrow 2_1^+)$ also allows for an important comparison to predictions made with recent shell-model calculations. A shell-model study with the SDPF-U-MIX effective interaction predicted the $B(E2; 4_1^+ \rightarrow 2_1^+)$ value for different pure configurations, finding $B(E2) = 16 e^2 \text{fm}^4$ for pure $0p0h$, $B(E2) = 107 e^2 \text{fm}^4$ for pure $2p2h$, and $B(E2) = 168 e^2 \text{fm}^4$ for pure $4p4h$ configurations [16]. Thus, a 4_1^+ lifetime measurement can be used to distinguish the collective mode of the ground-state band and constrain the underlying contributions from normal and intruder configurations.

To understand the collectivity in the ground-state band of ^{32}Mg , $B(E2)$ values of the 2_1^+ to 0_1^+ and 4_1^+ to 2_1^+ transitions have been determined using lifetime measurements. This article reports the lifetime measurements of the 2_1^+ state using the recoil-distance method [23] and the 4_1^+ state using the Doppler-shift attenuation method [25]. Both measurements were made simultaneously using the same experimental setup at the National Superconducting Cyclotron Laboratory (NSCL) Coupled Cyclotron Facility [26] with the S800

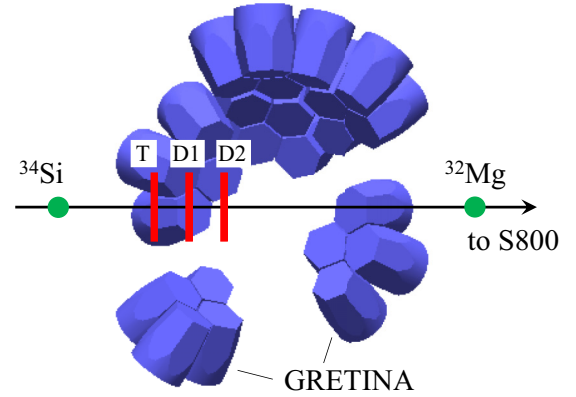


FIG. 1. The experimental setup in this work. GREYINA modules of high-purity Ge detectors surround the foils positioned by the TRIPLEX device. The target (T), first degrader (D1), and second degrader (D2) foils are shown (the size and separation of the foils are not to scale). The ^{34}Si secondary beam reacts on the foils and the ^{32}Mg reaction product leaves the target chamber and proceeds to the S800 spectrograph where it is identified.

spectrograph [27], the TRIPLE PLunger for EXotic Beams (TRIPLEX) device [28], and the Gamma-Ray Energy Tracking In-beam Nuclear Array (GREYINA) [29]. The $B(E2)$ values that result from these lifetime measurements are discussed and compared with theoretical predictions for the ground-state band in ^{32}Mg .

II. EXPERIMENT

This experiment was performed at the NSCL Coupled Cyclotron Facility [26] using a ^{48}Ca primary beam with an energy of 140 MeV/nucleon on a ^9Be production target. This resulted in a ^{34}Si secondary beam with an energy of 60 MeV/nucleon which was selected by the A1900 fragment separator [30] with a purity of 67%. The ^{34}Si secondary beam was directed to the target chamber in front of the S800 spectrograph [27]. Excited states of ^{32}Mg were populated in the $^9\text{Be}(^{34}\text{Si}, ^{32}\text{Mg})X$ reaction on a 52.9-mg/cm²-thick ^9Be target. Other reaction products were produced, including ^{30}Mg which is discussed later to confirm the analysis of the ^{32}Mg data set. Reaction products were identified by time-of-flight and energy-loss measurements from the S800 spectrograph.

GREYINA was used to detect γ rays emitted in flight by the ^{32}Mg reaction products and is depicted in the experimental setup shown in Fig. 1 [29]. GREYINA is composed of modules that each contain four independent high-purity Ge detectors. Each detector is electrically segmented and a signal decomposition is performed to provide precise position information for the γ -ray interaction which is critical for the proper correction of the Doppler-shift effect for γ rays emitted by in-flight ions. After including the ion trajectory information from the S800 spectrograph, GREYINA can achieve an in-beam γ -ray resolution of 1.1% at 1779 keV [29]. During this experiment, GREYINA was composed of ten modules. Four modules were placed at 58° , two at 90° , and four at

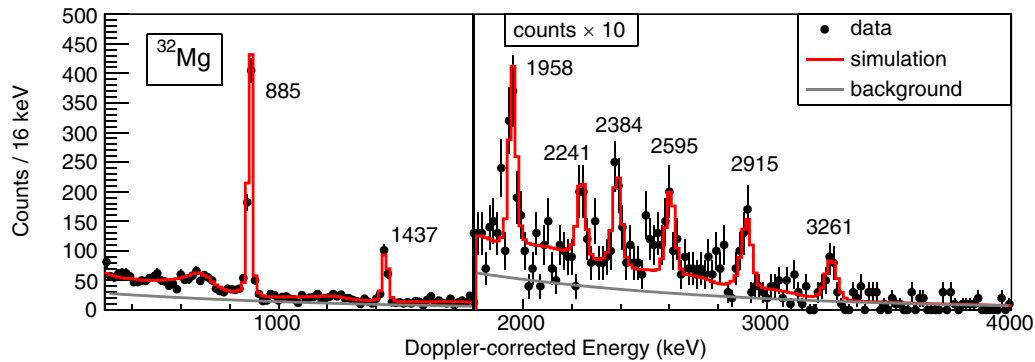


FIG. 2. A γ -ray spectrum observed in coincidence with ^{32}Mg reaction products with only the target foil T installed. The data are shown with black dots and error bars. The exponential background is shown with a solid gray line. The results of a GEANT4 simulation in addition to the background is shown with a solid red line that closely matches the data points.

122° relative to the beam axis measured from the center of GRETINA. Tracking and adback of the γ -ray interaction points were implemented in the same manner as described in Ref. [15].

The TRIPLEX device was used to position up to three foils in the target chamber as shown in Fig. 1 [28]. The first foil was the ^9Be target (T) with a thickness of 52.9 mg/cm^2 and was located 13 cm upstream of the center of GRETINA. The target was followed by two ^{181}Ta degraders at variable distances which are discussed below. The first degrader (D1) was 420 mg/cm^2 thick and the second degrader (D2) was 427 mg/cm^2 thick. A 7-mg/cm^2 -thick polyethylene foil was installed on the TRIPLEX device after the D2 foil to increase the proportion of fully stripped charge states accepted by the S800 spectrograph in the three-foil settings.

Using the three foils of the TRIPLEX device, the lifetimes of the 2_1^+ and the 4_1^+ states could be measured simultaneously despite the different lifetime ranges expected for the two states. To accomplish this, the T and D1 foils were in contact for the lifetime-measurement setting while the separation of the D1 and D2 foils was varied. Based on the previous experiments, the 2_1^+ lifetime is expected to be about $\tau(2_1^+) = 16(3)$ ps [24]. To be sensitive to that lifetime range with the recoil-distance method, the separation between the D1 and D2 foils was set to be 0.5, 0.7, 1.0, and 2.0 mm in four independent settings. These separations correspond to an ion travel time of approximately 5 to 20 ps between D1 and D2. The 4_1^+ lifetime was expected to be approximately $\tau(4_1^+) = 1$ ps. The T and D1 foils were placed in contact with each other, having a nominal separation of 0.0 mm so that the 4_1^+ lifetime could be measured simultaneously using the Doppler-shift attenuation method.

Extracting lifetime results requires an understanding of the feeding scheme that populates the states of interest. To quantify the amount of feeding from higher-lying states populated in the reaction, an additional experimental setting with only the target foil T installed on the TRIPLEX device was used.

In both lifetime methods used in this experiment, the lifetimes of states produced through reactions on the target foil T are measured by observing the various degrees of Doppler shift as the ions are slowed by passing through the degrader foils. However, reactions can take place on any of the three

foils installed in the TRIPLEX device during the experiment. To quantify reaction contributions from each of the degrader foils, another setting was implemented with a 25-mm separation between the T and D1 foils and a 22-mm separation between the D1 and D2 foils. With the large separations, each state that is populated in a reaction on a given foil decays before reaching the following foil. Therefore, it is possible to determine the relative number of reactions on each foil using this large-separation setting.

III. RESULTS

The following sections describe the results of the TRIPLEX settings that constrain crucial properties of ^{32}Mg and ultimately arrive at the lifetime results. First, the results of the target-only setting are used to determine the excited states populated in the reaction. Next, the three-foil setting with large separations is used to find the relative number of reactions that take place on each foil. Finally, the three-foil settings with small separations are used to determine the lifetimes of the 2_1^+ and 4_1^+ states.

A. ^{32}Mg excited states

The γ -ray spectrum obtained during the target-only setting is shown in Fig. 2. Since only one foil is in place, it is possible to cleanly resolve the γ -ray peaks corresponding to the depopulation of higher-lying states with relatively low intensity.

The peaks with the greatest intensity in Fig. 2 are the 885-keV and the 1437-keV peaks corresponding to the decays of the 2_1^+ and 4_1^+ states, respectively. Higher-lying states which decay to either the 2_1^+ or the 4_1^+ state were also observed with lower intensities. The γ -ray transitions and excited states in this work are displayed in the level scheme in Fig. 3 and listed in Table I, where the spin and parity of the states at higher energy than the 4_1^+ state are based on Ref. [24]. The transitions at 2241(4), 2595(6), and 2915(5) keV are consistent with γ rays observed in the past [4]. The 2241(4)-keV transition and the 2595(6)-keV transition observed here are consistent with the 2230(14)-keV and 2603(16)-keV transitions, respectively [4]. The 2915(5)-keV transition is closest to the previously observed 2883(16)-keV transition [4] and, while

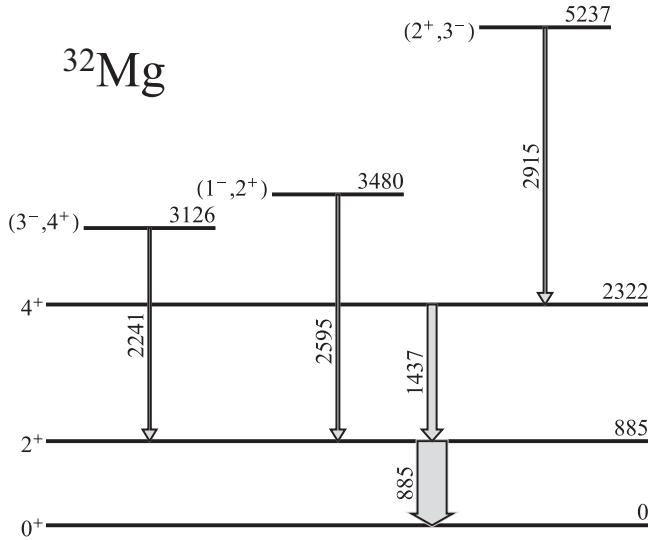


FIG. 3. A partial level scheme of ^{32}Mg showing the states and transitions observed in this work. The width of each arrow is proportional to the intensity of the transition.

the difference in energy is larger, it is still within 2σ standard error. Therefore, the 2915(5)-keV transition observed in this work is assumed to be the same as the 2883(16)-keV transition observed before.

The 3261(12)-keV transition observed in this work is consistent with the 3256(43)-keV peak-like structure observed in Ref. [4] in coincidence with the 885-keV transition. The 3256(43)-keV peak-like structure was omitted from the level scheme in Ref. [4] due to the lack of significant evidence for it in the singles spectrum and the coincidence spectrum with the 1437-keV transition. The 1958(4)-keV transition observed in this work is closest to the 1972.9(5)-keV transition from the published data [24,31]. The energies of these two transitions do not agree, so we conclude that the transition at 1958(4) keV is a newly observed transition. The transition

TABLE I. The excitation energy E_x , spin and parity J^π , lifetime τ , γ -ray transition energy E_γ , γ -ray intensity relative to the 885-keV transition I_γ , and transition final state E_f for the states of ^{32}Mg observed in this work. The final uncertainty is reported for the new lifetime and energy measurements where the statistical and systematic uncertainties have been added in quadrature. The spin and parity assignments are based on the results of past experiments.

E_x (keV)	J^π	τ (ps)	E_γ (keV)	I_γ	E_f (keV)
0	0_1^+				
885	2_1^+	18.9(14)	885.3(1) ^a	100	0
2322	4_1^+	0.9(2)	1436.8(4) ^a	31(5)	885
3126	$(3^-, 4^+)$		2241(4)	8.3(18)	885
3480	$(1^-, 2^+)$		2595(6)	10(3)	885
5237	$(2^+, 3^-)$		2915(5)	10(2)	2322
			1958(4)	15(3)	
			2384(4)	10(2)	
			3261(12)	7(2)	

^aValue taken from past measurements [24].

observed in this work at 2384(4) keV also does not agree with any other previously published transition to our knowledge and is considered to be new.

In the present experiment, the 1958-, 2384-, and 3261-keV transitions are in coincidence with the 885-keV transition. Therefore, the feeding of these transitions to the 2_1^+ state is included in our lifetime analysis. However, it is possible that the 1958-, 2384-, and 3261-keV transitions populate the 4_1^+ state or another higher-lying state that then decays to the 2_1^+ state, so these transitions are not assigned to a particular location in the level scheme in Fig. 3.

The target-only γ -ray spectrum was fit with the results of GEANT4 simulations [32] that incorporate the details of the experimental setup and are shown with a red line in Fig. 2. The scales of the simulations were fit to the observed peaks to deduce the intensities of the γ rays. The weighted averages of the past measurements of the $2_1^+ \rightarrow 0_1^+$ and $4_1^+ \rightarrow 2_1^+$ transitions are 885.3(1) and 1436.8(4) keV [24], respectively, and are precise enough for the sensitive lifetime measurements reported in this work. The energies of the higher-lying states can be obtained with better precision in this experiment than was possible in past experiments. The γ -ray energies and their intensities relative to the 885-keV transition are reported in Table I.

The transitions that feed the 2_1^+ and 4_1^+ states have an impact on the lifetime results. Although the γ -ray intensities and the feeding scheme are constrained, the lifetimes of the higher-lying states are experimentally unknown. Short feeding lifetimes of about $\tau \leq 0.1$ ps would have little effect on the lifetime results of the 2_1^+ state. Lifetimes of about $\tau = 1.0$ ps can have an effect in this experiment and ought to be accounted for. Using average reduced transition strengths observed in the $A = 30$ – 34 mass region as reported in Fig. 3 of Ref. [33], the partial lifetime of a state decaying by a particular electromagnetic transition can be estimated. The multipolarities of the higher-lying transitions in ^{32}Mg are not strictly known, but based on the range of values provided by different multipolarity assumptions, a reasonable estimate for the lifetimes of the higher-lying states can be found.

For the 2241-keV transition, the average transition strengths reported by Ref. [33] lead to a lifetime of the 3126-keV state of 0.056 ps if the 2241-keV transition is $M1$ isovector, 0.22 ps if it is $E1$ isovector, and 1.2 ps if it is $E2$ isoscalar. For the higher-energy transitions, the lifetime estimates decrease, such that for the 2915-keV transition, the 5237-keV state would have a lifetime of 0.026 ps if the 2915-keV transition is $M1$ isovector, 0.098 ps if it is $E1$ isovector, 0.32 ps if it is $E2$ isoscalar. Based on the current best estimates for spin and parity assignments, the 2595-keV transition can be either an $E1$ or $M1$ transition. The 2241- and 2915-keV transitions are likely to be either $E1$ or $E2$ transitions. The 1958-, 2384-, and 3261-keV transitions could possibly be $E1$, $M1$, or $E2$, but higher-order transitions would be unlikely.

For transitions that are of $E1$ or $M1$ multipolarity, the lifetimes of the higher-lying states are around 0.1 ps or less. For transitions of $E2$ multipolarity, the lifetimes of the higher-lying states are on the order of 1 ps. As a result, the lifetimes of the feeding states are all likely to be ≈ 1 ps or shorter. The effect of the unmeasured feeding state lifetimes on the

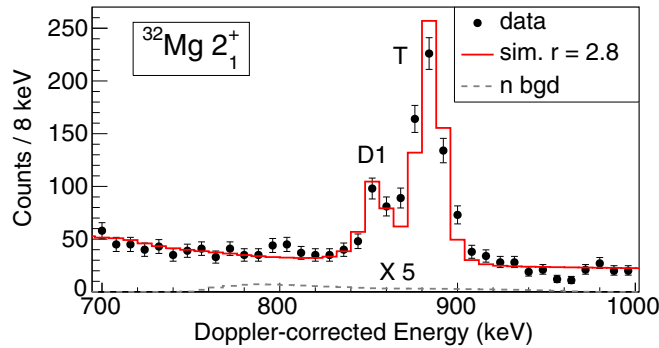


FIG. 4. A Doppler-shift-corrected γ -ray spectrum observed in coincidence with ^{32}Mg reaction products with all three foils installed with large separation in the TRIPLEX device. The 885-keV peak appears with two components corresponding to reactions on the target (T) and first degrader (D1) foils at a separation of 25 mm. The data (black dots and error bars) are fit with a simulation (solid red line). γ rays emitted at an angle $\theta < 70^\circ$ were considered. The contribution of neutron-induced background is scaled by $\times 5$ and is shown with a dashed gray line. The simulation that best fits the data assumes $r(2_1^+) = 2.8$, meaning there are 2.8 reactions on the target for every 1 reaction on the first degrader.

final results was evaluated by varying the lifetimes of the higher-lying states up to $\tau = 1.0$ ps. This effect is included in the final uncertainty in the lifetimes reported later.

B. ^{32}Mg reaction ratios

The relative number of reactions on each of the three foils that create the 2_1^+ state was found using the γ -ray spectrum in Fig. 4, and the relative number of reactions on each foil that create the 4_1^+ state was found using Fig. 5. These spectra were observed with all three foils installed on the TRIPLEX device with large separations of 25 mm between the target

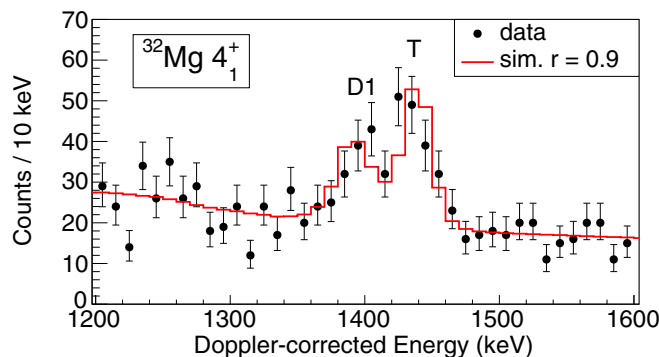


FIG. 5. A Doppler-shift corrected γ -ray spectrum observed in coincidence with ^{32}Mg reaction products with all three foils installed with large separation in the TRIPLEX device. The 1437-keV peak appears with two components corresponding to reactions on the target (T) and first degrader (D1) foils at a separation of 25 mm. The data (black dots and error bars) are fit with a simulation (red line). γ rays emitted at an angle $\theta < 70^\circ$ were considered. The simulation that best fits the data assumes $r(4_1^+) = 0.9$, meaning there are 0.9 reactions on the target for every 1 reaction on the first degrader.

foil T and the first degrader foil D1, and 22 mm between the first degrader D1 and the second degrader D2. Each γ -ray transition can have up to three components caused by decays occurring after each of the three foils with a different ion velocity. To resolve each peak component, the spectra are analyzed with a gate to select γ rays emitted at forward angles with a larger degree of Doppler shift. For Figs. 4 and 5, the angle gate was $\theta < 70^\circ$, which was found to be sufficiently forward-focused to resolve the peaks while still preserving a large enough number of events to have good statistics. Two components are observed in each spectrum corresponding to decays after the T and D1 foils. Since the separation between the foils is large compared with the distance the ion travels before decaying from the 2_1^+ or 4_1^+ state, the intensities of these peak components correspond to the number of reactions on the associated foil.

The S800 spectrograph did not accept all ^{32}Mg reaction products in the three-foil settings due to ions having momenta that was outside of the momentum acceptance of the S800. Significant portions of the ^{32}Mg reaction products produced on either the target foil T and the first degrader foil D1 were accepted by the S800, while for the second degrader foil D2 all ^{32}Mg reaction products had momenta that were too low to be accepted. As a result, there is no D2 component of the peaks in Figs. 4 and 5. The observed reaction product momentum distributions were reproduced in the simulation with proper cutoffs tuned to account for the S800 acceptance.

The reaction ratio for the 2_1^+ state was deduced from a χ^2 analysis to be $r(2_1^+) = 2.8(5)$, corresponding to 2.8 reactions populating the 2_1^+ state on the target foil T for every 1 reaction on the first degrader foil D1. The spectrum in Fig. 4 is fit with a GEANT4 simulation that assumes the reaction ratio value $r(2_1^+) = 2.8$ and is depicted with a red line. While the simulation shown in Fig. 4 does not pass through every data point in the peak region, the χ^2 distribution was well minimized at this value of $r(2_1^+)$. The displayed simulation is successful in reproducing the relative yield between the T and D1 components, which is the most critical factor in determining the $r(2_1^+)$ value.

Laboratory-frame γ -ray background from neutron-induced reactions in the detectors and surrounding materials has been found in the past to potentially cause an impact on γ -ray spectra with an angle gate [34,35]. The intensity of neutron-induced background in this experiment was estimated from the laboratory-frame γ -ray spectrum, then included in the corresponding ion-frame simulated spectrum in Fig. 4. For the contribution of this background to be visible, it was scaled by a factor of $\times 5$. This contribution was too small to have an impact on the $r(2_1^+)$ result. The neutron-induced background shown in Fig. 4 is the most intense background contribution that appears near the γ -ray energies of interest in any of the Doppler-shift corrected spectra shown in this work. For the remainder of the analysis presented in this article, the neutron-induced background was neglected.

The reaction ratio for the 4_1^+ state was deduced to be $r(4_1^+) = 0.9(2)$, corresponding to 0.9 reactions populating the 4_1^+ state on the target foil T for every 1 reaction on the first degrader foil D1. Figure 5 shows the GEANT4 simulation with a reaction ratio of $r(4_1^+) = 0.9$ depicted with a solid red line that

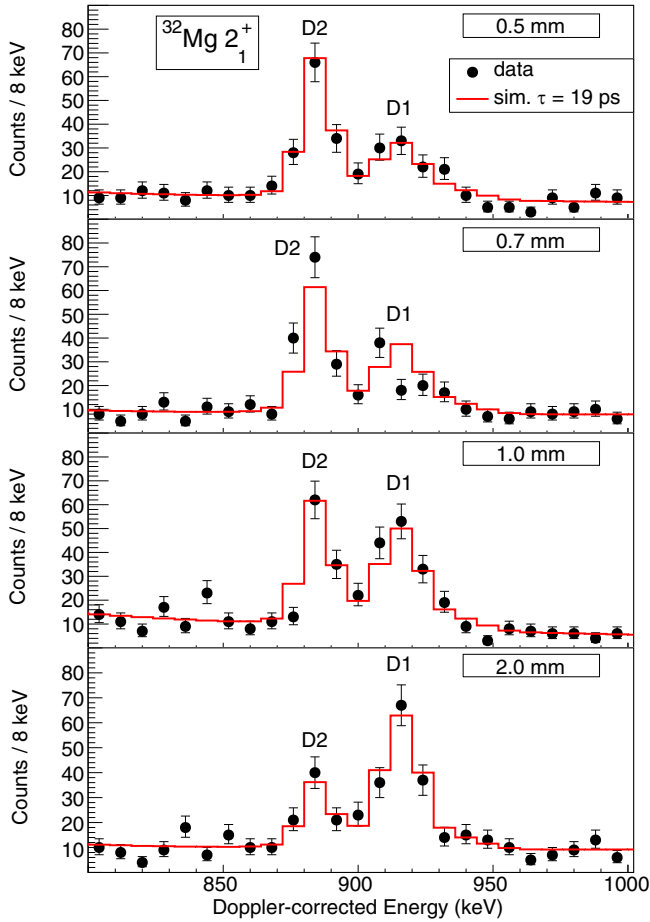


FIG. 6. Doppler-shift corrected γ -ray spectra observed in coincidence with ^{32}Mg reaction products showing the 885-keV peak from the four settings used to measure lifetimes. The target and first degrader foils were touching for all four settings, while the first and second degrader foils had a separation of 0.5, 0.7, 1.0, and 2.0 mm. γ rays emitted at an angle $\theta < 50^\circ$ were considered. The two peak components correspond to decays after the first degrader (D1) and second degrader (D2) foils, respectively. The data are shown with black dots and error bars, while a simulation result assuming a lifetime of $\tau(2_1^+) = 19$ ps is shown with a solid red line.

closely matches the experimental data. Note the considerable difference between $r(2_1^+)$ and $r(4_1^+)$. In general, the reaction ratio r depends on the final state of the reaction product. This is because the cross section of the final state depends on the nuclei present in the material that serves as a target for the reaction, which is ^9Be in the target foil and ^{181}Ta in the degrader foils. The difference in this experiment between $r(2_1^+)$ and $r(4_1^+)$ highlights this effect and emphasizes that the reaction ratio r ought to be determined for each state of interest in lifetime measurements with multiple foils of different materials.

C. The ^{32}Mg 2_1^+ lifetime

The 885-keV peak in ^{32}Mg is shown in Fig. 6 for the four settings used to measure lifetimes, separately. Two components of the 885-keV peak are visible in each spectrum: a fast

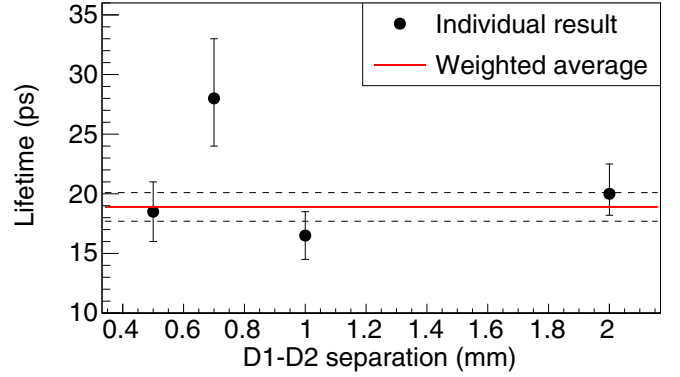


FIG. 7. The results for the 2_1^+ lifetime for each of the 0.5-, 0.7-, 1.0-, and 2.0-mm settings independently. The weighted average of the four settings is shown as a solid red line at $\tau(2_1^+) = 18.9$ ps. 1σ error bars are shown for the statistical uncertainty of each independent setting (black dots and error bars) and the final weighted average (dashed black horizontal lines).

component corresponding to decays after the first degrader foil D1, and a slow component corresponding to decays after the second degrader foil D2. The target and first degrader foils had zero separation, so a distinct component corresponding to decays after the target foil T does not appear. Note how as the separation between the D1 and D2 foils increases, the D1 component tends to increase, as expected. The solid red line in Fig. 6 corresponds to the results of GEANT4 simulations that assumed a lifetime of $\tau(2_1^+) = 19.0$ ps, near the final weighted average result found below.

Each setting in Fig. 6 was analyzed independently through a χ^2 analysis with GEANT4 simulations that vary the assumed 2_1^+ lifetime. Reasonable fits could be obtained from Fig. 6 for the 0.5-, 1.0-, and 2.0-mm settings. The 0.7-mm setting shows a D1 component that is slightly shifted relative to the other three settings and with a larger statistical fluctuation. Reasonable fits for the 0.7-mm setting were obtained with a coarser binning that increases the number of counts in each bin, reducing the effect of random statistical variations. Possible causes for the apparent variation in the 0.7-mm setting are discussed in the last paragraph of this section.

The four separate results from the 0.5-, 0.7-, 1.0-, and 2.0-mm settings are shown in Fig. 7 along with 1σ error bars from the statistical uncertainty. The final result is the weighted average of the four independent results $\tau(2_1^+) = 18.9 \pm 1.2(\text{stat.}) \pm 0.8(\text{syst.})$ ps. Note that there is no significant change in the weighted average lifetime if the 0.7-mm setting is excluded from the data set.

The largest source of systematic uncertainty is attributed to uncertainties in the feeding from the higher-lying states. In evaluating the lifetime, the feeding of the 2_1^+ state shown in Fig. 3 was implemented in the simulation, and the unplaced 1958-, 2384-, and 3261-keV transitions were included as feeding to the 2_1^+ state. The effective lifetime of the 4_1^+ state is constrained to be the value reported in the following section. The lifetimes of the other higher-lying states were varied from 0 to 1.0 ps, and the population of each state in the level scheme was varied while remaining consistent

with the measured intensities given in Table I. Due to the relatively small population of each of the feeding states, the effects of varying the feeding state lifetime by as much as 1.0 ps only causes an associated uncertainty in the 2_1^+ lifetime of 0.5 ps. The uncertainty in the intensities themselves contributed an uncertainty of 0.1 ps to the 2_1^+ lifetime. The separation between the D1 and D2 foils has an important role in the $\tau(2_1^+)$ measurement and contributes an uncertainty of 0.4 ps. Uncertainties in the ion velocity, position of the foils relative to GRETINA, separation between the T and D1 foils, and feeding were studied and found to each contribute 0.2 ps or less to the final uncertainty in $\tau(2_1^+)$. Each of these contributions added in quadrature led to the total systematic uncertainty of 0.8 ps.

As shown in Fig. 7, the setting with 0.7 mm of separation between the D1 and D2 foils does not agree within 1σ with the weighted average result. It is not too surprising that one out of the four settings yields a result that does not fall within 1σ since for a normal distribution the 1σ range should encompass only 68% of the independent results. Nevertheless, hypothetical causes of systematic error in the 0.7-mm setting were explored. Time-dependent changes in the beam intensity, purity, momentum distribution, and position distribution were investigated but were found to be insignificant and unable to explain the 0.7-mm lifetime discrepancy. During the experiment the separation between the foils was monitored with the linear actuator that positions the D2 foil, the position measurement of the micrometer, and by the induced voltage on the D2 foil due to a pulse applied to the D1 foil. These measurements all indicated that the foils were kept at a separation of 0.7 mm throughout the setting. Ruling out these possible causes for the deviation in the 0.7-mm setting, the most likely cause is the random fluctuations inherent to counting statistics.

D. The ^{32}Mg 4_1^+ lifetime

The 4_1^+ lifetime can be determined in this experiment with the Doppler-shift attenuation method by summing all four of the settings with different separations between the D1 and D2 foils while the T and D1 foils remained in contact. The 1437-keV peak observed with the T and D1 foils in contact is shown in Fig. 8. The 4_1^+ state is short-lived so when it is populated from reactions on the T and D1 foils, it will decay within those foils, and the 4_1^+ state will not decay past the D2 foil which never comes closer than 0.5 mm to the D1 foil.

The 4_1^+ lifetime was found through a χ^2 analysis between the data and GEANT4 simulations by varying the lifetime of the 4_1^+ state. The lifetime result is $\tau(4_1^+) = 0.9 \pm 0.2(\text{stat.}) \pm 0.1(\text{syst.})$ ps. For comparison, simulation results that assume a 4_1^+ lifetime of 0.3, 0.9, and 1.5 ps are shown in Fig. 8. The 0.3 ps lifetime assumption results in a spectrum that overpredicts the counts on the high-energy side of the 1437-keV peak and underpredicts the counts on the low-energy side of the peak. This is consistent with the expectation that, for a shorter lifetime, more decays will occur further upstream in the T and D1 foils where the ion is traveling at a higher speed. The 1.5 ps lifetime assumption has the inverse problem: it underpredicts the counts in the high-energy side

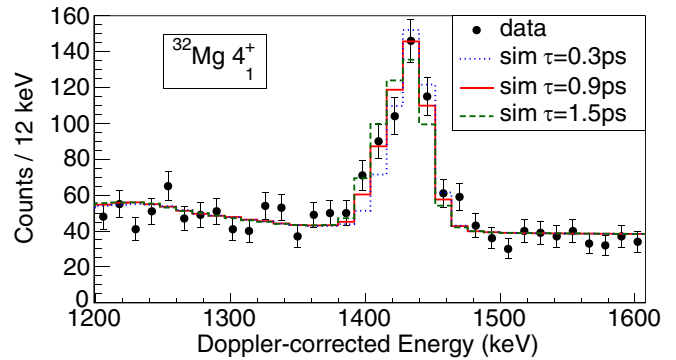


FIG. 8. A Doppler-shift corrected γ -ray spectrum showing the 1437-keV peak from the decay of the 4_1^+ state of ^{32}Mg . The spectrum is the sum of all runs where the target and first degrader foils were touching, regardless of the separation between the first and second degrader foils. γ rays emitted at an angle $\theta < 70^\circ$ were considered. The data are shown with black dots and error bars, while the closest simulation result with a lifetime of $\tau(4_1^+) = 0.9$ ps is shown with a solid red line. For comparison, a simulation with a lifetime of 0.3 ps is shown with a dotted blue line and a simulation with a lifetime of 1.5 ps is shown with a dashed green line.

of the peak and overpredicts the counts in the low-energy side of the peak.

The lifetimes of the states feeding the 4_1^+ state are unknown and could plausibly be as long as the 4_1^+ lifetime, so the measurement presented here is the effective lifetime τ of the 4_1^+ state. The largest sources of systematic uncertainty are due to the uncertainty in the separation between the target and first degrader foils, and the uncertainty in the reaction ratio $r(4_1^+)$. Each of these components caused an uncertainty in the $\tau(4_1^+)$ lifetime of 0.1 ps or less, resulting in a final systematic uncertainty of 0.1 ps when added in quadrature.

E. The ^{30}Mg 2_1^+ lifetime

The analysis of the ^{32}Mg 4_1^+ lifetime can be validated by using the same approach on a complementary data set. In the same experimental setup, ^{30}Mg reaction products were produced from reactions of the ^{34}Si secondary beam on the ^9Be target foil. The 2_1^+ state of ^{30}Mg has an adopted lifetime of 2.2(3) ps and an energy of $E_x = 1483$ keV [36], making it an excellent case for the Doppler-shift attenuation method that was used with the ^{32}Mg 4_1^+ state.

Following the same approach used for the ^{32}Mg results, the first step is to constrain the feeding of the 2_1^+ state of ^{30}Mg . There were too few counts of ^{30}Mg in the target-only setting to determine which excited states were populated. Instead, the three-foil large separation setting was used, and this γ -ray spectrum is shown in Fig. 9. Two peaks were observed in coincidence with the ^{30}Mg reaction products which correspond to the $2_1^+ \rightarrow 0_1^+$ transition of 1483 keV and the $4_1^+ \rightarrow 2_1^+$ transition of 1898 keV. Both peaks have only one component which corresponds to reactions on the target foil T. All ^{30}Mg reaction products produced on the first degrader foil D1 or the second degrader foil D2 had momenta that were too low to be accepted by the S800 spectrograph. Therefore, it was

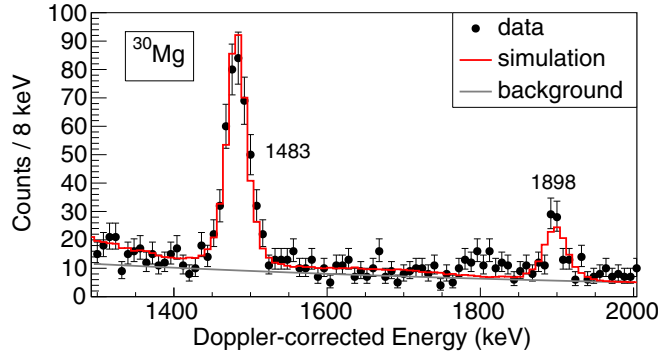


FIG. 9. A Doppler-shift-corrected γ -ray spectrum in coincidence with ^{30}Mg reaction products in the three-foil, large separation setting. The data are shown with black dots and error bars. The GEANT4 simulation result is shown with a solid red line, and the exponential background is shown with a solid gray line. No gate was placed on the γ -ray emission angle θ . Two peaks are seen corresponding to the decays of the 2_1^+ and 4_1^+ states. Both peaks have only one component corresponding to reactions on the target foil.

not necessary to determine the reaction ratio r for any of the states in ^{30}Mg . From Fig. 9, it was found that the intensity of the 1898-keV transition was 33(7)% relative to the 1483-keV transition.

All the data collected with the T and D1 foils in contact were summed and are shown in Fig. 10 for the ^{30}Mg reaction products. A lineshape corresponding to the decays of the 2_1^+ state in the T and D1 foils can be seen. The data are compared with simulation results that assume various lifetimes. One can see that the lifetime result of $\tau = 2.3$ ps matches the lineshape well. A longer lifetime such as $\tau = 3.1$ ps tends to overpredict the yield in the low-energy side of the peak, while a shorter lifetime of $\tau = 1.5$ ps has too little yield in the low-energy side of the peak. From the χ^2 analysis, the lifetime

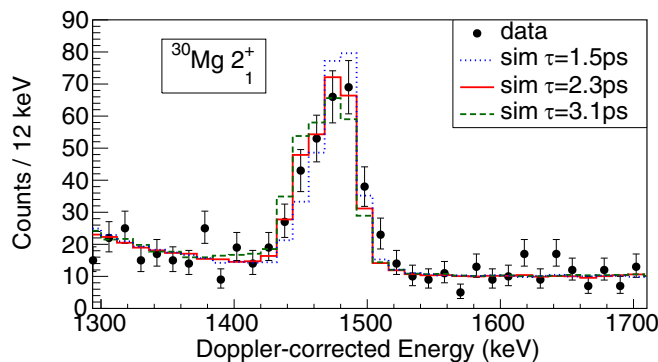


FIG. 10. A Doppler-shift corrected γ -ray spectrum in coincidence with ^{30}Mg reaction products in the three-foil settings with zero separation between the T and D1 foils. γ rays emitted at an angle $\theta < 50^\circ$ were considered. The peak at 1483 keV corresponds to the decay of the 2_1^+ state. The data (black dots with error bars) is matched well with the simulation results that assume a lifetime of 2.3 ps (solid red line). For comparison the simulation results are shown for a lifetime of 1.5 ps (dotted blue line) and 3.1 ps (dashed green line).

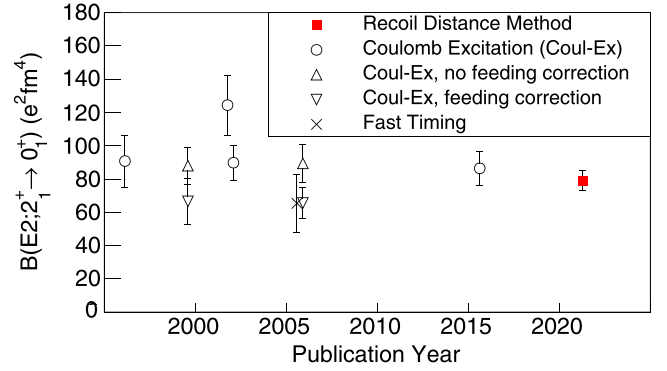


FIG. 11. The $B(E2; 2_1^+ \rightarrow 0_1^+)$ value in ^{32}Mg reported in experiments over the past few decades. The present recoil-distance method result is shown with a red square. The Coulomb-excitation measurements from Refs. [6,8,9,11] are shown with open circles. The open triangles are the results from Refs. [7,10]. The upward-pointing triangles reflect the $B(E2)$ values without feeding corrections while the corresponding downward-pointing triangles take into account feeding corrections. The saltire symbol (\times) represents the fast-timing measurement of Ref. [12].

result was found to be $\tau(2_1^+) = 2.3 \pm 0.3(\text{stat.}) \pm 0.1(\text{syst.})$ ps which leads to a reduced transition rate of $B(E2; 2_1^+ \rightarrow 0_1^+) = 49(7) e^2 \text{fm}^4$. This present lifetime result is remarkably consistent with the adopted lifetime value of 2.2(3) ps [36]. Due to the match between the present result and the past result for the 2_1^+ lifetime in ^{30}Mg , the result given in the previous section for the lifetime of the 4_1^+ state in ^{32}Mg can be taken with confidence.

IV. DISCUSSION

In this section we report the $B(E2)$ values in ^{32}Mg determined from the lifetimes measured in this work. Comparisons are made between the experimental values and theoretical predictions. The $B(E2; 2_1^+ \rightarrow 0_1^+)$ value in ^{32}Mg is discussed first. Then, a discussion of the $B(E2; 4_1^+ \rightarrow 2_1^+)$ value follows.

A. ^{32}Mg $B(E2; 2_1^+ \rightarrow 0_1^+)$

The lifetime measurement from the present experiment is $\tau(2_1^+) = 18.9 \pm 1.2(\text{stat.}) \pm 0.8(\text{syst.})$ ps and results in $B(E2; 2_1^+ \rightarrow 0_1^+) = 79(6) e^2 \text{fm}^4$, or $B(E2; 0_1^+ \rightarrow 2_1^+) = 395(30) e^2 \text{fm}^4$, which has better precision than any of the previous $B(E2)$ measurements. The $B(E2; 2_1^+ \rightarrow 0_1^+)$ result from this work is compared with past experimental results in Fig. 11.

The $B(E2)$ value from the present experiment is slightly lower but in good agreement with the adopted value which is $B(E2; 2_1^+ \rightarrow 0_1^+) = 91(13) e^2 \text{fm}^4$ [24]. This difference can be caused by unobserved feeding. Feeding corrections were made in the Coulomb excitation studies of Refs. [6–8,10,11]. However, additional unobserved feeding in the Coulomb excitation studies would cause the $B(E2)$ result to be higher than the true value, while in lifetime studies unobserved feeding causes the $B(E2)$ result to be lower. In the present study, unobserved feeding of the 2_1^+ state does not have a strong

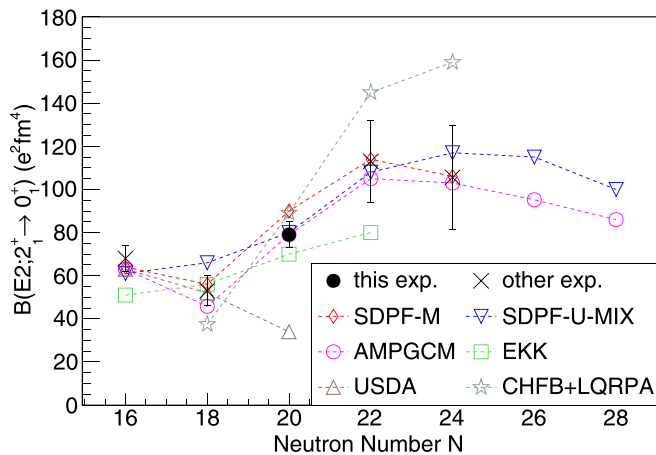


FIG. 12. The $B(E2; 2_1^+ \rightarrow 0_1^+)$ values in the Mg isotopic chain from ^{28}Mg to ^{40}Mg . The present ^{32}Mg result is shown with a filled black circle. The experimental values from other results are shown with black saltires (\times) and are from Refs. [36–39]. Theoretical calculations are also shown for the SDPF-M [18] (red line and open diamonds), SDPF-U-MIX [16] (blue line and open inverted triangles), AMPGCM [19,20] (purple line and open circles), EKK [22] (emerald green line and open squares), USDA [40] (brown line and open triangles), and CHFb + LQRPA calculations [21] (sage green line and open stars).

impact on the reported $B(E2)$ value. In the ^{32}Mg 2_1^+ lifetime analysis, the feeding scheme shown in Fig. 3 was used, and the 1958-, 2384-, and 3261-keV transitions which could not be definitely placed in the level scheme were included in the feeding correction as if they directly feed the 2_1^+ state. By summing the intensities for feeders in Table I, the feeding corrections accounted for 81% of the 2_1^+ decays. The remaining 19% of the 2_1^+ decays are due to direct population of the 2_1^+ state or unobserved feeding, establishing an upper limit to the possible unobserved feeding. Even if we assume the maximum amount of unobserved feeding is present and that the unobserved feeding states have a lifetime of 1 ps, the 2_1^+ lifetime result from this experiment does not significantly change.

To interpret the present $B(E2; 2_1^+ \rightarrow 0_1^+)$ value, it is compared with theoretical predictions for the $B(E2; 2_1^+ \rightarrow 0_1^+)$ value in ^{32}Mg and other even-even Mg isotopes [36–39] in Fig. 12. The USDA shell-model calculation uses only sd -shell orbitals for the valence space for both protons and neutrons and does not agree with the $B(E2; 2_1^+ \rightarrow 0_1^+)$ for ^{32}Mg [40]. Shell-model calculations that include pf orbitals in the valence space such as the SDPF-M [18] and SDPF-U-MIX [16] calculations can incorporate the 2p2h and 4p4h intruder configurations and are successful in reproducing the increase in $B(E2; 2_1^+ \rightarrow 0_1^+)$ along the Mg isotopes that begins at ^{32}Mg . The angular-momentum-projected generator coordinate method (AMPGCM) follows an approach based on a mean-field calculation and agrees well with the available $B(E2; 2_1^+ \rightarrow 0_1^+)$ data across the Mg isotopes [19,20]. The AMPGCM result suggests significant mixing of both oblate and prolate configurations in the ground-state band of ^{32}Mg . The constrained Hartree-Fock-Bogoliubov plus local

QRPA (CHFb + LQRPA) result [21] solves a microscopically derived five-dimensional quadrupole collective Schrödinger equation to obtain the states of ^{32}Mg and is suitable for describing a variety of collective phenomena. The CHFb + LQRPA calculation concurs with the interpretation of deformation in the ground state of ^{32}Mg . The extended Kuo-Krenciglowa (EKK) result is the most recent and is closely tied to microscopic theory to derive effective interactions [22]. The EKK result finds that ^{32}Mg is dominated by intruder configurations in the ground-state band but also suggests that ^{30}Mg has large contributions from intruder configurations as well.

The calculations that include the deformation-driving intruder configurations from the pf shell succeed in reproducing the increase in $B(E2)$ from ^{30}Mg to ^{32}Mg that is demonstrated in the data [16,18–22]. For ^{32}Mg , the present result for the $B(E2; 2_1^+ \rightarrow 0_1^+)$ value is best reproduced by the SDPF-U-MIX and AMPGCM calculations. Taken together, the theoretical calculations seem to indicate that the ground-state band is dominated by deformation-driving intruder configurations, involving both the 2p2h and 4p4h configurations.

B. ^{32}Mg $B(E2; 4_1^+ \rightarrow 2_1^+)$

This experiment was the first to measure the lifetime of the 4_1^+ state of ^{32}Mg and obtained a result of $\tau(4_1^+) = 0.9 \pm 0.2(\text{stat.}) \pm 0.1(\text{syst.})$ ps. The corresponding reduced transition strength is $B(E2; 4_1^+ \rightarrow 2_1^+) = 148_{-30}^{+47} e^2 \text{fm}^4$. This result is based on an effective lifetime of the 4_1^+ state, but if the true lifetime is shorter, then the resulting $B(E2; 4_1^+ \rightarrow 2_1^+)$ would become larger. The large $B(E2; 4_1^+ \rightarrow 2_1^+)$ value is a signature of the large collectivity of this transition. This underscores the breaking of the $N = 20$ magic number and confirms the continuation of large collectivity to higher spin in the ground-state band of ^{32}Mg . The spin-parity assignment of the 4_1^+ state was previously made from a proton-scattering experiment [4]. This $B(E2; 4_1^+ \rightarrow 2_1^+)$ value supports the 4_1^+ assignment and the interpretation of this band as collective in nature.

The $B(E2)$ predictions for the 2_1^+ to 0_1^+ and the 4_1^+ to 2_1^+ transitions in ^{32}Mg using the SDPF-U-MIX calculation with pure 0p0h, 2p2h, and 4p4h configurations were reported in Ref. [16] (Fig. 1 of that article). As the calculation goes from pure 0p0h to 2p2h to 4p4h configurations, the $B(E2)$ value is predicted to increase for both transitions. The present $B(E2; 2_1^+ \rightarrow 0_1^+)$ result of $79(6) e^2 \text{fm}^4$ is close to the pure 2p2h prediction of $83 e^2 \text{fm}^4$. However, the present $B(E2; 4_1^+ \rightarrow 2_1^+)$ result of $148_{-30}^{+47} e^2 \text{fm}^4$ is larger than the pure 2p2h prediction of $107 e^2 \text{fm}^4$ and instead agrees best with the pure 4p4h prediction of $168 e^2 \text{fm}^4$. The consistency of the pure 2p2h calculation with the $2_1^+ \rightarrow 0_1^+$ transition and the pure 4p4h calculation with the $4_1^+ \rightarrow 2_1^+$ transition suggests that the relative contribution of the 2p2h and 4p4h intruder configurations changes significantly with spin. The ratio of $B(E2)$ values for the $4_1^+ \rightarrow 2_1^+$ and $2_1^+ \rightarrow 0_1^+$ transitions can now be deduced from the results of this experiment. The energy ratio $E(4_1^+)/E(2_1^+)$

TABLE II. The energy and $B(E2)$ ratios observed for ^{32}Mg and predicted from several models.

^{32}Mg	$E(4_1^+)/E(2_1^+)$	$\frac{B(E2;4_1^+ \rightarrow 2_1^+)}{B(E2;2_1^+ \rightarrow 0_1^+)}$
Data	2.61	$1.9^{+0.6}_{-0.4}$
Vibrator	2.0	2.0
Symmetric rotor	3.33	1.43
EKK [22]	2.55	1.37
CHFB + LQRPA [21]	2.82	1.76

and $B(E2)$ ratio $B(E2;4_1^+ \rightarrow 2_1^+)/B(E2;2_1^+ \rightarrow 0_1^+)$ for ^{32}Mg are shown in Table II along with available predicted values. The energy ratio $E(4_1^+)/E(2_1^+)$ agrees best with the EKK calculation, however the $B(E2)$ ratio does not. The CHFB + LQRPA calculation does well at reproducing both ratios. The energy and $B(E2)$ results appear to suggest that the simple paradigms of vibrational or symmetric rotational modes are insufficient to describe the ground-state band in ^{32}Mg . However, the $B(E2)$ ratio has a large uncertainty which is mostly due to uncertainty in the 4_1^+ lifetime measurement. The short lifetime of the 4_1^+ state is near the limit of sensitivity for the present experimental setup with fast rare-isotope beams. A dedicated Doppler-shift attenuation method measurement at a lower beam energy would likely be able to measure the 4_1^+ lifetime with higher precision.

V. CONCLUSION

This work simultaneously measured the lifetimes of the 2_1^+ and 4_1^+ states of ^{32}Mg with the recoil-distance method and Doppler-shift attenuation method, respectively. The combination of techniques highlights the flexibility of the TRIPLEX device in facilitating lifetime measurement experiments with rare-isotope beams. The 2_1^+ lifetime yields the most precise experimental $B(E2;2_1^+ \rightarrow 0_1^+)$ value in ^{32}Mg yet and offers a resolution to disagreements among the past experimental results. The 4_1^+ lifetime reported here is the first known lifetime measurement for that state. The results indicate the presence of large collectivity driven by intruder configurations in the ground-state band of ^{32}Mg , while the normal configuration is less involved. The data also suggest that the configuration-mixing among the 2p2h and 4p4h configurations is not static but changes with spin in the ground-state band of ^{32}Mg .

ACKNOWLEDGMENTS

This work was supported by the U.S. Department of Energy (DOE), Office of Science, Office of Nuclear Physics, under Grant No. DE-SC0020451, the U.S. National Science Foundation (NSF) under Grant No. PHY-1565546, and by the DOE National Nuclear Security Administration through the Nuclear Science and Security Consortium, under Award No. DE-NA0003180. GRETINA was funded by the DOE, Office of Science. Operation of the array at NSCL was supported by DOE under Grants No. DE-SC0014537 (NSCL) and No. DE-AC02-05CH11231 (LBNL).

-
- [1] E. K. Warburton, J. A. Becker, and B. A. Brown, *Phys. Rev. C* **41**, 1147 (1990).
- [2] C. Détraz, M. Langevin, M. C. Goffri-Kouassi, D. Guillemaud, M. Epherre, G. Audi, C. Thibault, and F. Touchard, *Nucl. Phys. A* **394**, 378 (1983).
- [3] C. Détraz, D. Guillemaud, G. Huber, R. Klapisch, M. Langevin, F. Naulin, C. Thibault, L. C. Carraz, and F. Touchard, *Phys. Rev. C* **19**, 164 (1979).
- [4] S. Takeuchi, N. Aoi, T. Motobayashi, S. Ota, E. Takeshita, H. Suzuki, H. Baba, T. Fukui, Y. Hashimoto, K. Ieki, N. Imai, H. Iwasaki, S. Kanno, Y. Kondo, T. Kubo, K. Kurita, T. Minemura, T. Nakabayashi, T. Nakamura, T. Okumura *et al.*, *Phys. Rev. C* **79**, 054319 (2009).
- [5] H. L. Crawford, P. Fallon, A. O. Macchiavelli, A. Poves, V. M. Bader, D. Bazin, M. Bowry, C. M. Campbell, M. P. Carpenter, R. M. Clark, M. Cromaz, A. Gade, E. Ideguchi, H. Iwasaki, C. Langer, I. Y. Lee, C. Loelius, E. Lunderberg, C. Morse, A. L. Richard *et al.*, *Phys. Rev. C* **93**, 031303(R) (2016).
- [6] T. Motobayashi, Y. Ikeda, Y. Ando, K. Ieki, M. Inoue, N. Iwasa, T. Kikuchi, M. Kurokawa, S. Moriya, S. Ogawa, H. Murakami, S. Shimoura, Y. Tanagisawa, T. Nakamura, Y. Watanabe, M. Ishihara, T. Teranishi, H. Okuno, and R. F. Casten, *Phys. Lett. B* **346**, 9 (1995).
- [7] B. V. Pritychenko, T. Glasmacher, P. D. Cottle, M. Fauerback, R. W. Ibbotson, K. W. Kemper, V. Maddalena, A. Navin, R. Ronningen, A. Sakharuk, H. Scheit, and V. G. Zelevinsky, *Phys. Lett. B* **461**, 322 (1999).
- [8] V. Chisté, A. Gillibert, A. Leépine-Szily, N. Alamanos, F. Auger, J. Barrette, F. Braga, M. D. Cortina-Gil, Z. Dlouhy, V. Lapoux, M. Lewitowicz, R. Lichtenthaler, R. L. Neto, S. M. Lukyanov, M. MacCormick, F. Marie, W. Mittig, F. de Oliveira Santos, N. A. Orr, A. N. Ostrowski *et al.*, *Phys. Lett. B* **514**, 233 (2001).
- [9] H. Iwasaki, T. Motobayashi, H. Sakurai, K. Yoneda, T. Gomi, N. Aoi, N. Fukuda, Z. Fülöp, U. Futakami, Z. Gacsi, Y. Higurashi, N. Imai, N. Iwasa, T. Kubo, M. Kunibu, M. Kurokawa, Z. Liu, T. Minemura, A. Saito, M. Serata *et al.*, *Phys. Lett. B* **522**, 227 (2001).
- [10] J. A. Church, C. M. Campbell, D.-C. Dinca, J. Enders, A. Gade, T. Glasmacher, Z. Hu, R. V. F. Janssens, W. F. Mueller, H. Olliver, B. C. Perry, L. A. Riley, and K. L. Yurkewicz, *Phys. Rev. C* **72**, 054320 (2005).
- [11] K. Li, Y. Ye, T. Motobayashi, H. Scheit, P. Doornenbal, S. Takeuchi, N. Aoi, M. Matsushita, E. Takeshita, D. Pang, and H. Sakurai, *Phys. Rev. C* **92**, 014608 (2015).
- [12] H. Mach, L. M. Fraile, O. Tengblad, R. Boutami, C. Jollet, W. A. Plóciennik, D. T. Yordanov, M. Stanoiu, M. J. G. Borge, P. A. Butler, J. Cedarkäll, P. Fogelberg, H. Fynbo, P. Hoff, A. Jokinen, A. Korgul, U. Köster, W. Kurcewicz, F. Marechal, T. Motobayashi *et al.*, *Eur. Phys. J. A* **25**, 105 (2005).
- [13] K. Wimmer, T. Kröll, R. Krücken, V. Bildstein, R. Gernhäuser, B. Bastin, N. Bree, J. Diriken, P. Van Duppen, M. Huysse, N. Patronis, P. Vermaelen, D. Voulot, J. Van de Walle, F. Wenander,

- L. M. Fraile, R. Chapman, B. Hadinia, R. Orlandi, J. F. Smith *et al.*, *Phys. Rev. Lett.* **105**, 252501 (2010).
- [14] A. O. Macchiavelli, H. L. Crawford, C. M. Campbell, R. M. Clark, M. Cromaz, P. Fallon, M. D. Jones, I. Y. Lee, M. Salathe, B. A. Brown, and A. Poves, *Phys. Rev. C* **94**, 051303(R) (2016).
- [15] R. Elder, H. Iwasaki, J. Ash, D. Bazin, P. C. Bender, T. Braunroth, B. A. Brown, C. M. Campbell, H. L. Crawford, B. Elman, A. Gade, M. Grindler, N. Kobayashi, B. Longfellow, A. O. Macchiavelli, T. Mijatović, J. Pereira, A. Revel, D. Rhodes, J. A. Tostevin *et al.*, *Phys. Rev. C* **100**, 041301(R) (2019).
- [16] E. Caurier, F. Nowacki, and A. Poves, *Phys. Rev. C* **90**, 014302 (2014).
- [17] N. Fukunishi, T. Otsuka, and T. Sebe, *Phys. Lett. B* **296**, 279 (1992).
- [18] Y. Utsuno, T. Otsuka, T. Mizusaki, and M. Honma, *Phys. Rev. C* **60**, 054315 (1999).
- [19] R. R. Rodríguez-Guzmán, J. L. Egido, and L. M. Robledo, *Phys. Rev. C* **62**, 054319 (2000).
- [20] R. Rodríguez-Guzmán, J. Egido, and L. Robledo, *Nucl. Phys. A* **709**, 201 (2002).
- [21] N. Hinohara, K. Sato, K. Yoshida, T. Nakatsukasa, M. Matsuo, and K. Matsuyanagi, *Phys. Rev. C* **84**, 061302(R) (2011).
- [22] N. Tsunoda, T. Otsuka, N. Shimizu, M. Hjorth-Jensen, K. Takayanagi, and T. Suzuki, *Phys. Rev. C* **95**, 021304(R) (2017).
- [23] A. Dewald, O. Möller, and P. Petkov, *Prog. Part. Nucl. Phys.* **67**, 786 (2012).
- [24] C. Ouellet and B. Singh, *Nucl. Data Sheets* **112**, 2199 (2011).
- [25] P. J. Nolan and J. F. Sharpey-Schafer, *Rep. Prog. Phys.* **42**, 1 (1979).
- [26] A. Gade and B. M. Sherrill, *Phys. Scr.* **91**, 053003 (2016).
- [27] D. Bazin, J. A. Caggiano, B. M. Sherrill, J. Yurkon, and A. Zeller, *Nucl. Instrum. Methods Phys. Res., Sect. B* **204**, 629 (2003).
- [28] H. Iwasaki, A. Dewald, T. Braunroth, C. Fransen, D. Smalley, A. Lemasson, C. Morse, K. Whitmore, and C. Loelius, *Nucl. Instrum. Methods Phys. Res., Sect. A* **806**, 123 (2016).
- [29] D. Weisshaar, D. Bazin, P. C. Bender, C. M. Campbell, F. Recchia, V. Bader, T. Baugher, J. Belarge, M. P. Carpenter, H. L. Crawford, M. Cromaz, B. Elman, P. Fallon, A. Forney, A. Gade, J. Harker, N. Kobayashi, C. Langer, T. Lauritsen, I. Y. Lee *et al.*, *Nucl. Instrum. Methods Phys. Res., Sect. A* **847**, 187 (2017).
- [30] D. J. Morrissey, B. M. Sherrill, M. Steiner, A. Stolz, and I. Wiedenhoever, *Nucl. Instrum. Methods Phys. Res., Sect. B* **204**, 90 (2003).
- [31] V. Tripathi, S. L. Tabor, P. Bender, C. R. Hoffman, S. Lee, K. Pepper, M. Perry, P. F. Mantica, J. M. Cook, J. Pereira, J. S. Pinter, J. B. Stoker, D. Weisshaar, Y. Utsuno, and T. Otsuka, *Phys. Rev. C* **77**, 034310 (2008).
- [32] S. Agostinelli, J. Allison, K. Amako, J. Apostolakis, H. Araujo, P. Arce, M. Asai, D. Axen, S. Banerjee, G. Barrand, F. Behner, L. Bellagamba, J. Boudreau, L. Broglia, A. Brunengo, H. Burkhardt, S. Chauvie, J. Chuma, R. Chytracsek, G. Cooperman *et al.*, *Nucl. Instrum. Methods Phys. Res., Sect. A* **506**, 250 (2003).
- [33] P. M. Endt, *At. Data Nucl. Data Tables* **55**, 171 (1993).
- [34] C. Loelius, H. Iwasaki, B. A. Brown, M. Honma, V. M. Bader, T. Baugher, D. Bazin, J. S. Berryman, T. Braunroth, C. M. Campbell, A. Dewald, A. Gade, N. Kobayashi, C. Langer, I. Y. Lee, A. Lemasson, E. Lunderberg, C. Morse, F. Recchia, D. Smalley *et al.*, *Phys. Rev. C* **94**, 024340 (2016).
- [35] C. Loelius, N. Kobayashi, H. Iwasaki, D. Bazin, J. Belarge, P. C. Bender, B. A. Brown, R. Elder, B. Elman, A. Gade, M. Grindler, S. Heil, A. Hufnagel, B. Longfellow, E. Lunderberg, M. Mathy, T. Otsuka, M. Petri, I. Syndikus, N. Tsunoda *et al.*, *Phys. Rev. Lett.* **121**, 262501 (2018).
- [36] M. S. Basunia, *Nucl. Data Sheets* **111**, 2331 (2010).
- [37] M. S. Basunia, *Nucl. Data Sheets* **114**, 1189 (2013).
- [38] N. Nica and B. Singh, *Nucl. Data Sheets* **113**, 1563 (2012).
- [39] P. Doornenbal, H. Scheit, S. Takeuchi, N. Aoi, K. Li, M. Matsushita, D. Steppenbeck, H. Wang, H. Baba, E. Ideguchi, N. Kobayashi, Y. Kondo, J. Lee, S. Michimasa, T. Motobayashi, A. Poves, H. Sakurai, M. Takechi, Y. Togano, and K. Yoneda, *Phys. Rev. C* **93**, 044306 (2016).
- [40] B. A. Brown and B. H. Wildenthal, *Annu. Rev. Nucl. Part. Sci.* **38**, 29 (1988).